Diffusivity of Carbon Dioxide in Molten Salts

Eizo Sada,* Shigeo Katoh, Hidehumi Yoshii, and Kiyoshi Yasuda

Chemical Engineering Department, Kyoto University, Kyoto 606, Japan

The diffusion coefficients of carbon dioxide in molten $NaNO_3$ and a eutectic mixture of lithium and potassium chlorides were determined by measuring gas absorption rates from rising bubbles in the molten salts. The diffusion coefficient in molten $NaNO_3$ at 350 °C was higher than those of the eutectic mixture at 450 and 530 °C.

In recent years molten salts have been used in chemical and atomic industries. Little is known, however, about the diffusivity in molten salts except for the self-diffusion coefficients of ions measured by use of tracer-diffusion or electrochemical methods. Although it is necessary to measure the diffusion coefficients of gases in molten salts in investigating kinetics of gas–molten salt reactions, diffusion measurements have so far been limited to diffusion coefficients of gases by use of the polarographic method (*2*, *10*). In the present work, diffusion coefficients of carbon dioxide in molten sodium nitrate and a eutectic mixture of lithium and potassium chlorides were determined by measuring gas absorption rates from rising bubbles in the molten salts.

Experimental Section

Figure 1 shows one of the four absorbers used in the present work. Each absorber, made of Pyrex glass, was equipped with a coaxial inner tube of 5-mm inside diameter, through which gas bubbles rose from a bubbling tube, of 3-mm inside diameter, at the bottom. A nitrogen inlet, a gas outlet, and a thermocouple holder were inserted through the cap of the absorber. To evaluate the end effects associated with bubble formation and rupture, we used different lengths of inner tubes for the four absorbers (H in Figure 1): 6, 8, 10, and 12 cm. The distance between the top of the inner tube and the cap of the absorber was the same in all of the absorbers. The surface of molten salts was adjusted to ca. 5 mm above the top of the inner tube.

The molten salts used were $NaNO_3$ and a eutectic mixture of LiCl (58 mol %)–KCl (42 mol %). The salts were of reagent grade and were dried in a desiccator for a few days and in a vacuum oven at 150 ~ 200 °C for several hours.

Figure 2 is a schematic diagram of the entire apparatus. A weighed quantity of the salt was transferred to the absorber, melted at a desired temperature, and dried again by bubbling anhydrous nitrogen through the bubbling tube for 1 h. The drying precedure in this work may be considered to be adequate because samples of the eutectic mixture dried by bubbling hydrogen chloride prior to drying with nitrogen showed the same absorption rates of carbon dioxide as samples dried by the above-mentioned procedure. The temperature of the furnace was measured with a chromel–alumel thermocouple inserted into the molten salt and kept constant within ±5 °C.

Carbon dioxide (superpure grade, 99.96% and free from water) was preheated through a stainless steel tube wound with a flexible insulated heater and bubbled into the molten salt through the bubbling tube at a constant flow rate for a predetermined time. Long capsule-shaped bubbles of carbon dioxide, ca. 2.2 cm in length and 0.47 cm in diameter, rose through the inner tube one by one at a constant frequency, and carbon dioxide was absorbed into the molten salt. The frequency of bubble formation was counted visually. The bubble length was measured from photographs taken with an electronic flash, and the rising velocity of the bubble was determined by analyzing 16-mm movie films. Figure 3 is a typical photograph of a rising bubble.

After absorption of carbon dioxide, the gas supply line to the bubbling tube was swept with nitrogen until all carbon dioxide had been displaced. The bubbling tube was also washed by supplying five bubbles to the tube. Then nitrogen was introduced through the nitrogen inlet for 3 min at a flow rate of 44 cm^3/min to sweep the head space of the absorber. Losses of absorbed carbon dioxide during these procedures were estimated to be less than 3% of the total amount.

Carbon dioxide absorbed in the salt was eluted by bubbling nitrogen through the bubbling tube at a flow rate of 17.5 cm^3/min. The concentration of carbon dioxide in the eluted gas was measured with an infrared carbon dioxide analyzer (Shimadzu, Type URA-2s) and was recorded continuously. The amount of carbon dioxide absorbed in the salt was obtained by graphical integration of the concentration of carbon dioxide multiplied by the flow rate of eluted gas. Since the vapor pressures of these salts were very low in the temperature range used, the effect of the vapor pressure was neglected.

The carbon dioxide balance gives

$$V\frac{dC}{dt} = K_L a'(C^* - C) \tag{1}$$

where $K_L a'$ is the volumetric coefficient of liquid-phase mass transfer. Integration gives

$$V \ln C^*/(C^* - C_t) = K_L a' t \tag{2}$$

where C_t is the absorbed carbon dioxide concentration at time t and C^* is the value of C in equilibrium with 1 atm of carbon dioxide. The values of C^* in molten $NaNO_3$ and the eutectic mixture of LiCl–KCl were measured by the same elution method as in the previous paper (*6*). The $K_L a'$ value was determined from the slope of a $V \ln C^*/(C^* - C_t)$ vs. t plot for each run.

The volumetric coefficient $K_L a'$ involves the end effects associated with bubble formation and rupture. Irrespective of the height of the inner tube, the contribution of these effects to $K_L a'$ should be equal because of the similar construction of the four absorbers, provided the length of the inner tube exceeds that required for a rising bubble to reach a constant velocity. Thus, the volumetric coefficient can be separated into two terms

$$K_L a' = k_L a + k_{L,END} a'' \tag{3}$$

The first term is associated with gas absorption from the bubble rising at constant velocity, and the second with gas absorption at bubble formation and rupture.

Based on the penetration theory (*3*), the liquid-phase mass transfer coefficient k_L in eq 3 can be expressed by eq 4. When

$$k_L = 2[D_L/(\pi t)]^{1/2} \tag{4}$$

the liquid film on the inner tube wall around the rising bubble is substantially stationary, the gas–liquid contact time t of the liquid film can be expressed by eq 5 (*3*), where h and u_b are the length

$$t = h/u_b \tag{5}$$

and the constant velocity of the rising bubble. From eq 4 and 5

$$k_L = 2[D_L u_b/(\pi h)]^{1/2} \tag{6}$$

0021-9568/80/1725-0341$01.00/0

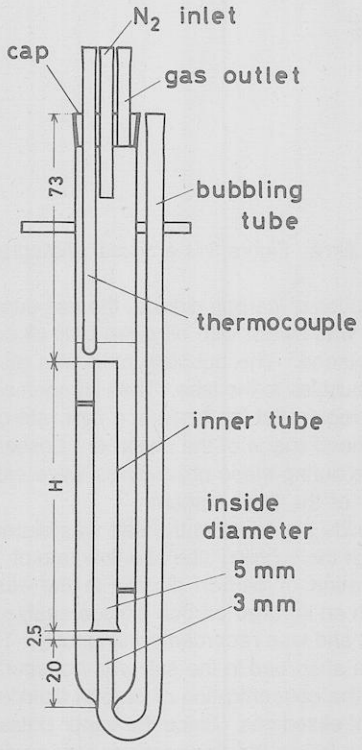

Figure 1. Absorber.

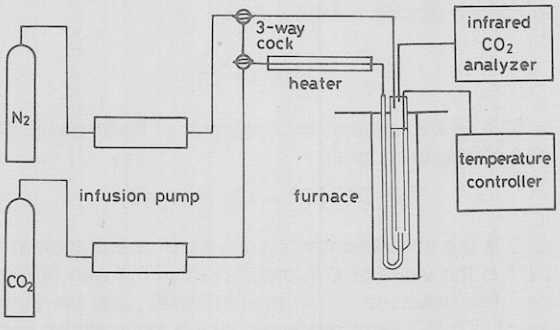

Figure 2. Schematic diagram of experimental setup.

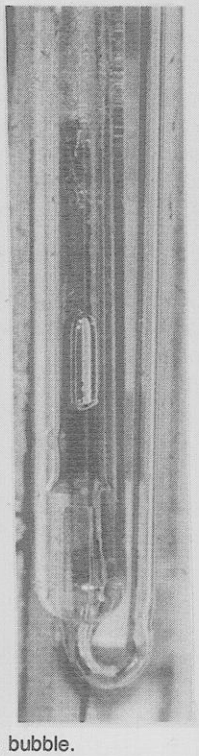

Figure 3. Typical rising bubble.

Table I. Physical Properties of Molten Salts

salt	temp, °C	density, g/cm³	surface tension, g/s²	viscosity, g/(cm s)	solubility of CO_2, mol/(cm³ atm)
$NaNO_3$	350	1.888	114.7	2.32×10^{-2}	1.1×10^{-6}
LiCl–KCl (58 mol %–42 mol %)	450	1.647	130.0	2.55×10^{-2}	2.4×10^{-6}
LiCl–KCl (58 mol %–42 mol %)	530	1.606	123.4	1.96×10^{-2}	3.0×10^{-6}

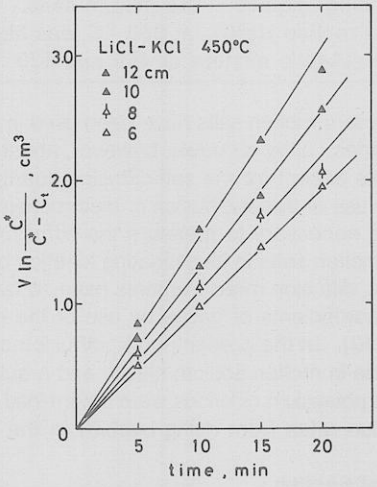

Figure 4. Plots for evaluation of K_La'.

The gas–liquid interfacial area a of the bubble rising at the constant velocity can be calculated by representing the bubble by two hemispheres joined by a cylinder

$$a = [4\pi r^2 + 2\pi r(h - 2r)]n(H - H')/u_b \qquad (7)$$

where n is the frequency of bubble formation, and H' the inner tube height at which the rising bubble reaches the constant velocity. Substituting eq 6 and 7 into eq 3, one can obtain eq 8. Since H' may be considered constant irrespective of the

$$K_La' = 4nr(H - H')(\pi hD_L/u_b)^{1/2} + k_{L,END}a'' \qquad (8)$$

length H of the inner tube, a plot of K_La' vs. H gives a straight line. The slope of the straight line is

$$\lambda = 4nr(\pi hD_L/u_b)^{1/2} \qquad (9)$$

Thus, the diffusion coefficient can be obtained as

$$D_L = \frac{\lambda^2 u_b}{16\pi n^2 r^2 h} \qquad (10)$$

Results and Discussion

The physical properties of the molten salts used in this work are shown in Table I. For a given value of K_La', a plot of the left-hand side of eq 2 against time t from the start of a run should give a straight line, from the slope of which K_La' can be evaluated. Figure 4 shows the $V \ln C^*/(C^* - C_t)$ vs. t plots for the runs with the LiCl–KCl eutectic at 450 °C. Similar plots were obtained with data from other runs.

Figure 5 shows the K_La' values for $NaNO_3$ and LiCl–KCl plotted against the length of the inner tube. From the slopes of the straight lines and observed values of u_b, n, h, and r, the diffusion coefficients of carbon dioxide in these molten salts can be obtained. These values are summarized in Table II. The errors in the diffusivity measurement arose mainly in the determination of the slope λ, the error in which was doubled in calculating diffusivity from eq 10. So the accuracy of the dif-

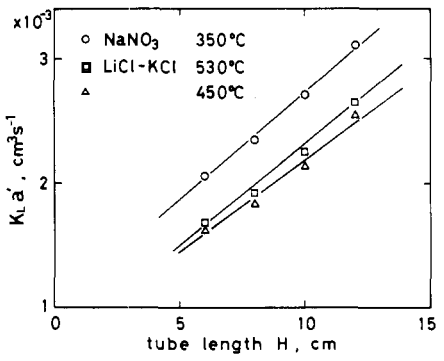

Figure 5. Values of $K_L a'$ plotted against tube length.

Table II. Observed Values

system	temp, °C	u_b, cm/s	h, cm	r, cm	n, 1/s	diffusivity of CO_2, cm^2/s
$NaNO_3$	350	29.8	2.13	0.235	0.075	2.53×10^{-5}
LiCl-KCl (58 mol %-42 mol %)	450	27.3	2.21	0.236	0.083	1.32×10^{-5}
LiCl-KCl (58 mol %-42 mol %)	530	30.2	2.26	0.234	0.087	1.70×10^{-5}
water	20	27.1	2.10	0.237	0.083	1.86×10^{-5}

fusion coefficients was estimated to be ±30%.

To determine the reliability of the equipment and procedure, we measured the diffusion coefficient of carbon dioxide in pure water at 20 °C by a method similar to that used for the molten salts. The value shown in Table II agreed well with the value of 1.66×10^{-5} cm^2/s in the literature (*8*).

The diffusion coefficient in the LiCl–KCl eutectic increases with temperature, but even at 530 °C it is smaller than that in $NaNO_3$ at 350 °C. The bulky shape of the NO_3^- ion might be responsible for the higher diffusivity of carbon dioxide in molten $NaNO_3$. These values of the gas diffusivity are of the same order as the self-diffusion coefficients of ions in molten salts. For example, the self-diffusion coefficient of Na^{22} in $NaNO_3$ at 365 °C is 2.53×10^{-5} cm^2/s (*7*).

Several factors might affect the accuracy of the experimental data. One is the state of the liquid film on the tube wall around the rising bubble, which can be analyzed by the theory of vertical slug flow in a liquid (*9*). The movement of a slug is governed by bouyancy, viscosity, and surface tension. According to Bretherton (*1*), surface tension dominates when the Eötvös number is smaller than 3.37, i.e.

$$N_{E\ddot{o}} = \frac{gd^2(\rho_l - \rho_g)}{\sigma} < 3.37 \qquad (11)$$

In this case, the results for horizontal slug flow are approximately valid for vertical flow, and the liquid film around the slug is substantially stationary (*9*). Since in the present experiments surface tension virtually dominated, and the effects due to gas viscosity and inertia were considered to be negligible, the liquid film on the tube wall around the rising bubble may be considered to be substantially stationary. Thus, the gas–liquid contact time is given by eq 5.

The thickness of the liquid film was ca. 0.015 cm. The penetration distance of carbon dioxide into the film within the gas–liquid contact time was estimated to be 50 μm. Thus, the effect of the tube wall on the penetration rate was negligible.

The concentration of carbon dioxide in the salts was considered to be almost uniform in view of the sufficient circulation caused by the rising bubbles. Since the length, the frequency, and the constant velocity of the rising bubble were independent of the length of the inner tube, and the rising bubble reached the constant velocity 3 cm above the bubbling tube, the slopes of plots in Figure 5 are independent of end effects.

Glossary

a	gas–liquid interfacial area, cm^2
C	dissolved carbon dioxide concentration, mol/cm^3
D_L	diffusivity of carbon dioxide in liquid, cm^2/s
d	diameter of tube, cm
g	gravitational constant, cm/s^2
H	length of inner tube, cm
h	length of bubble, cm
$K_L a'$	volumetric coefficient of liquid-phase mass transfer, cm^3/s
k_L	liquid-phase mass transfer coefficient, cm/s
$k_{L,END}a''$	volumetric coefficient associated with end effects, cm^3/s
$N_{E\ddot{o}}$	Eötvös number = $gd^2(\rho_l - \rho_g)/\sigma$
n	frequency of bubble formation, 1/s
r	bubble radius, cm
t	time, s
u_b	bubble velocity, cm/s
V	liquid volume, cm^3

Greek Letters

λ	slope defined by eq 9, cm^2/s
ρ_l	liquid density, g/cm^3
ρ_g	gas density, g/cm^3
σ	surface tension, g/s^2

Literature Cited

(1) Bretherton, F. P. *J. Fluid Mech.* **1961**, *10*, 166.
(2) Comtat, M.; Vothi, N. D. *J. Chim. Phys. Phys.-Chim. Biol.* **1976**, *73*, 109.
(3) Higbie, R. *Trans. Am. Inst. Chem. Eng.* **1935**, *31*, 365.
(4) Janz, G. J. "Molten Salt Handbook"; Academic Press: New York, 1967; pp 63–79.
(5) Janz, G. J.; Tomkins, R. P. T.; Allen, C. B.; Downey, J. R., Jr.; Gardner, G. L.; Krebs, U.; Singer, S. K. *J. Chem. Eng. Ref. Data* **1975**, *4*, 871.
(6) Sada, E.; Katoh, S.; Beniko, H.; Yoshii, H.; Kayano, M. *J. Chem. Eng. Data* **1980**, *25*, 45.
(7) Spedding, P. L.; Mills, R. *J. Electrochem. Soc.* **1965**, *112*, 594.
(8) Tang, Y. P.; Himmelblau, D. M. *AIChE J.* **1963**, *9*, 630.
(9) Wallis, G. B. "One Dimensional Two-Phase Flow"; McGraw-Hill, New York, 1969; pp 282–304.
(10) Zambonin, P. G.; Cardetta, V. L.; Signorile, G. *J. Electroanal. Chem.* **1970**, *28*, 237.

Received for review April 21, 1980. Accepted July 16, 1980. This work was supported financially by the Ministry of Education of Japan through a Grant-in-Aid for Special Project Research.